

Ziv-Zakai-Optimal OFDM Resource Allocation for Time-of-Arrival Estimation

Andrew M. Graff*, Todd E. Humphreys†

**Department of Electrical and Computer Engineering, The University of Texas at Austin*

†*Department of Aerospace Engineering and Engineering Mechanics, The University of Texas at Austin*

Abstract—This paper presents methods of optimizing the placement and power allocations of pilots in an orthogonal frequency-division multiplexing (OFDM) signal to minimize time-of-arrival (TOA) estimation errors under power and resource allocation constraints. TOA errors in this optimization are quantified through the Ziv-Zakai bound (ZZB), which captures error thresholding effects caused by sidelobes in the signal's autocorrelation function (ACF) which are not captured by the Cramer-Rao lower bound. This paper is the first to solve for these ZZB-optimal allocations in the context of OFDM signals, under integer resource allocation constraints, and under both coherent and noncoherent reception. Under convex constraints, the optimization of the ZZB is proven to be convex; under integer constraints, the optimization is lower bounded by a convex relaxation and a branch-and-bound algorithm is proposed for efficiently allocating pilot resources. These allocations are evaluated by their ZZBs and ACFs, compared against a typical uniform allocation, and deployed on a software-defined radio TOA measurement platform to demonstrate their applicability in real-world systems.

Index Terms—OFDM; positioning; Ziv-Zakai; convex optimization.

I. INTRODUCTION

Demand for accurate positioning services is growing rapidly. As next-generation networks continue to trend toward denser deployments and wider bandwidths, they have garnered increased interest as a provider of positioning services, both as a precise alternative to global navigation satellite system services and as an enabler of key environment-aware features in future 6G networks. Existing networks operate almost ubiquitously through orthogonal frequency-division multiplexing (OFDM), permitting positioning signals to be multiplexed with communications data across both time and frequency resources. These positioning resources, henceforth referred to as pilot resources, are known by users within the network, allowing receivers to correlate against the pilot resources to obtain time-of-arrival (TOA) estimates for use in several positioning protocols. Wireless networks face the difficult task of balancing the allocation of resources between these two services, with positioning users demanding more precise localization, and communications users demanding faster data rates. In such dual-functional networks, positioning signals that achieve optimal localization performance while subject to power and resource constraints are desirable. This paper explores the optimal allocation of pilot resources in an OFDM signal to minimize TOA errors subject to these constraints.

TOA estimation at the receiver is the first step in several positioning protocols including pseudorange multilateration,

time-difference-of-arrival, or round-trip-time, all of which have seen widespread use in existing cellular networks [1], [2]. To obtain a TOA estimate, the receiver may correlate delayed copies of the known pilot signal against the received signal, creating a correlation function. The receiver may then estimate the TOA relative to its local clock as the delay corresponding to the peak power of this correlation function. In an OFDM signal, the presence of the cyclic prefix allows this time-delay correlation to be computed as a frequency domain correlation that is orthogonal to subcarriers not modulated with pilot resources [3], assuming sufficiently small Doppler. As a result, the autocorrelation function (ACF) of the OFDM pilot signal depends only on the placement and power allocations of the pilot resources and not the phases of the pilot resources.

The shape of the ACF is of particular interest because it regulates how TOA estimation errors change with the signal-to-noise ratio (SNR). The ACF is typically described by its mainlobe, which is the correlation power near the true TOA; its sidelobes, which are spikes in correlation power occurring outside of the mainlobe; and grating lobes, which are images of the mainlobe caused by aliasing within the ACF. At high SNR, estimation errors tend to be concentrated near the peak of the mainlobe. As SNR decreases, however, it becomes increasingly likely that errors occur on sidelobes, which causes a sudden and drastic increase in estimation error variance due to their distance from the mainlobe. This phenomenon is referred to as the “thresholding effect,” which has been widely studied in TOA estimation [4]–[6] and motivated the use of the Barankin bound [7], [8] and the Ziv-Zakai bound (ZZB) [9] as alternatives to the Cramer-Rao lower bound (CRLB), which does not capture this effect. Large errors may also be introduced by grating lobes. If the duration of delays over which the receiver correlates is greater than the unambiguous region of the ACF, aliasing will occur and grating lobe ambiguities may appear in the correlation function that are indistinguishable from the mainlobe. Since the grating lobes are equally-powered images of the mainlobe, these errors occur irrespective of the SNR.

A pilot resource allocation designed for TOA estimation must account for all of these sources of error. Existing techniques typically transmit positioning signals that have power uniformly distributed over the spectrum, such as the positioning reference signal (PRS) in LTE and 5G NR. While these power allocations create sufficiently low sidelobes in the ACF, alternative power allocations may achieve lower TOA error variances when restricted to the same power budget

and signal bandwidth. The optimal allocation to minimize estimation error variance must balance the sharpness of the mainlobe against the sidelobe level and ensure that grating lobes are not present over the range of possible correlation delays. With *a priori* knowledge of both the receiver's SNR and the distribution of the TOA dictating the range of correlation delays, optimal allocations could significantly reduce TOA estimation errors without increasing the power budget or signal bandwidth. These allocations may also be designed to use a limited number of subcarriers, allowing networks to keep unused resources available for communications purposes. Furthermore, the receiver may perform either coherent correlation if the carrier phase is known accurately or noncoherent correlation otherwise, causing changes to the shape of the ACF and the distribution of post-correlation noise, thereby affecting the optimal allocation.

This paper optimizes the allocation of OFDM pilots to minimize the error variance of TOA estimates obtained from the OFDM signal, quantified through the ZZB. The optimization of the ZZB for TOA estimation has been discussed in prior work but never solved for the important class of OFDM signals, restricted to integer resource constraints, nor generalized to both coherent and noncoherent reception.

The ZZB is first expressed for OFDM signals under both coherent and noncoherent reception. In both the coherent and noncoherent cases, the minimization of the ZZB with respect to pilot power allocations while subject to a total power constraint is then proven to be a convex problem with readily calculated gradients, permitting efficient selection of optimal allocations. This minimization is then further constrained to only allocate power in a fixed number of subcarriers, yielding an integer-constrained problem that is lower-bounded by a convex relaxation. A branch-and-bound algorithm is then proposed, allowing approximately optimal allocations to be computed efficiently. Optimal (and approximately optimal) allocations are found over a range of SNRs for both the coherent and noncoherent versions of the convex-constrained and the integer-constrained problems. These allocations are then analyzed through their TOA error bounds and ACFs. Finally, to demonstrate their real-world applicability, TOA errors are measured on an software-defined radio (SDR) ranging platform transmitting OFDM signals generated from these allocations.

A. Prior Work

Prior work has analyzed signals for TOA estimation with theoretical bounds such as the ZZB and CRLB. The CRLB is derived to analyze the performance of TOA estimation with OFDM signals in [10] and [11]. Meanwhile, the ZZB on TOA estimation is derived under a tapped delay line channel model with statistical channel knowledge at the receiver for frequency-hopping signals [12] and for ultrawide bandwidth signals [13]. In the context of localization, the authors of [14] derive the ZZB on the positioning error of direct position estimation and two-step estimation based on TOA measurements. The ZZB on TOA estimation is also derived in the context of compressed sensing radar in [15]. While these studies provide

insights into TOA estimation errors from these bounds, they do not consider the optimal design of the signals to minimize TOA error.

Other prior work has used the CRLB, ZZB, and other criteria to optimize signal design for TOA estimation. The ZZB on TOA has been evaluated for sets of parametric candidate OFDM power allocations in [16]–[20], showing how allocating power toward the extremities of the band increases TOA precision in the high-SNR regime at the expense of high sidelobe levels and how power can be intelligently allocated to balance this tradeoff. However, none of these papers determine optimal power allocations and are restricted to the coherent ZZB, limiting applicability in practical systems where the carrier phase is unknown. Similarly, Wirsing et al. evaluate how different $\frac{\pi}{4}$ -QPSK signaling patterns affect the coherent ZZB [21].

The TOA ZZB is optimized in [22] to create SNR-adaptive waveforms subject to a power and bandwidth constraint, proving convexity of the phase-coherent ZZB with respect to a signal's ACF and demonstrating that notable reductions in TOA error are possible through Ziv-Zakai optimization. The optimization, however, does not consider the noncoherent ZZB, restrictions to OFDM signals, or the more complex resource constraints addressed in the current paper. Sun et al. [23] optimize the balance of power between positioning and communications signals to maximize data rate subject to a TOA error constraint using the ZZB, but only optimize for the total signal powers and do not optimize the allocation of power across frequency.

The design of a multiband OFDM signal is addressed in [24], where a sparse selection of bands is optimized subject to a TOA error variance constraint quantified by the CRLB with results verified on an SDR testbed. Multi-carrier power allocations are optimized using the CRLB to minimize TOA error for signal's experiencing interference using the CRLB in [25] and to minimize both TOA error and channel estimation error in [26], [27]. Li et al. optimize subcarrier power allocations in an OFDM integrated sensing and communications (ISAC) system to minimize the CRLB on ranging TOA estimation subject to power and minimum capacity constraints [28]. While the optimized signals in [24]–[28] may be effective in high SNR conditions, these designs are inapt at low SNRs due to their use of the CRLB. A weighted integrated sidelobe level optimization is conducted in [29] to design signals with desirable autocorrelation properties for TOA estimation in frequency-selective fading channels.

Outside of TOA estimation, the ZZB has also seen use in the context of multiple-input multiple-output (MIMO) radar. The noncoherent ZZB was used in [30] as a metric to evaluate sparse array designs for angle-of-arrival (AOA) estimation. The authors of [31] also derived the ZZB for the joint estimation of the position and velocity of targets in a MIMO radar system.

Beyond signal design for TOA estimation and positioning, a large body of prior work optimizes signal design for ISAC [32] and joint communications and sensing (JCAS) systems that focus on radar as the sensing component. Many of these ISAC studies have specifically considered the optimization

of OFDM waveforms and power allocations. The studies in [33]–[35] consider OFDM ISAC systems and optimize the transmitted signal using objective functions based on the sensing mutual information. The authors of [36] optimize the symbols of an OFDM ISAC system on resources allocated for radar sensing to minimize the CRLB on target TOA and Doppler estimation. Similarly, Wang et al. optimize subcarrier resource allocations and powers in a multicarrier ISAC system to maximize capacity while enforcing a minimum signal-to-interference-and-noise ratio (SINR) constraint for radar sensing, proposing a branch-and-bound algorithm for solving the allocation problem [37]. Ni et al. optimize the precoders of an OFDM JCAS system based on the SINR, radar mutual information, and radar CRLBs on delay, gain, and angle-of-departure [38]. Considering only an OFDM radar system, Sen et al. propose a multiobjective optimization to design subcarrier weights in OFDM radar waveforms to balance both sparse estimation error and detection performance [39]. This work on the optimization of OFDM ISAC and radar systems motivates the importance of optimized OFDM signal design. However, this work does not address the optimization of OFDM signals to minimize the ZZB on TOA estimation.

B. Contributions

The main contributions of this paper are as follows:

- Expressions for the ZZB on TOA estimation error variance for OFDM signals under both coherent and noncoherent reception.
- Proofs of the convexity of both the coherent and noncoherent ZZBs with respect to subcarrier power allocations.
- A branch-and-bound algorithm for efficiently albeit approximately solving the ZZB minimization problem under additional integer resource constraints on pilot resource allocation.
- Analysis of the optimal (and approximately optimal) pilot allocations, ACFs, and TOA error variances obtained from both the convex-constrained and integer-constrained problems under both coherent and noncoherent reception.
- Evaluation of the TOA error variance measured on an SDR platform transmitting OFDM signals using the optimized pilot allocations in comparison against an OFDM signal with a uniform pilot power allocation.

The remainder of the paper is organized as follows. Section II introduces the signal model, maximum-likelihood TOA estimators, ACFs, and error bounds on TOA estimation. Section III introduces the optimization problems. Section III-A frames the optimization under convex constraints, proves convexity, and derives expressions for gradients. Section III-B frames the optimization under integer constraints and proposes a branch-and-bound algorithm to efficiently solve for approximately-optimal allocations. Section IV analyzes the optimized allocations, ACFs, and ZZBs, comparing the results against a uniform allocation. Section V analyzes the performance of the optimized allocations on an SDR platform. Finally, Sec. VI ends the paper with conclusions drawn from the results.

Notation: Column vectors are denoted with lowercase bold, e.g., \mathbf{x} . Matrices are denoted with uppercase bold, e.g., \mathbf{X} . Scalars are denoted without bold, e.g., x . The i th entry of a vector \mathbf{x} is denoted $x[i]$ or in shorthand as x_i . The Euclidean norm is denoted $\|\mathbf{x}\|$. Real transpose is represented by the superscript T and conjugate transpose by the superscript H . The Q-function is denoted as $Q(\cdot)$. The Marcum-Q function of order ν is denoted as $Q_\nu(\cdot)$. The modified Bessel function of the first kind is denoted as $I_n(\cdot)$. Zero-based indexing is used throughout the paper; e.g., $x[0]$ refers to the first element of \mathbf{x} .

II. SIGNAL MODEL

Consider an OFDM signal with K subcarriers, a subcarrier spacing of Δ_f Hz, and a payload $x[k]$ for subcarrier indices $k \in \mathcal{K}$, where $\mathcal{K} = \{0, 1, \dots, K-1\}$. Let $d[k]$ be the mapping from subcarrier indices to physical distances in frequency from the carrier in units of subcarriers. This map is defined as $d[k] = k$ for $k = 0, 1, \dots, \frac{K}{2} - 1$ and $d[k] = k - K$ for $k = \frac{K}{2}, \frac{K}{2} + 1, \dots, K-1$. This signal propagates through an additive white Gaussian noise (AWGN) channel at a carrier frequency f_c and experiences a gain in signal power g , time delay τ_0 , phase shift ϕ_0 , and AWGN $v[k] \sim \mathcal{CN}(0, \sigma^2)$. The baseband received signal $y[k]$ is modeled in the frequency domain as

$$y[k] = \alpha[k]x[k] + v[k], \quad (1)$$

$$\alpha[k] = \sqrt{g} \exp(-j2\pi d[k]\Delta_f\tau_0 + j\phi_0). \quad (2)$$

This model assumes that the receiver begins sampling the transmitted OFDM symbol during the cyclic prefix, permitting the receiver to process the signal in the frequency domain.

Assuming that the payload $x[k]$ is fully known to the receiver, the receiver can obtain a maximum-likelihood estimate of τ_0 from the frequency domain correlation of $y[k]$ and $x[k]$. Let τ be the time delay at which the correlation function is evaluated. Through the remainder of this paper, this time delay will be normalized by the OFDM sampling period $T_s = \frac{1}{K\Delta_f}$ to define $z \triangleq \frac{\tau}{T_s}$. The true delay τ_0 is also scaled, defining $z_0 \triangleq \frac{\tau_0}{T_s}$. The complex correlation as a function of z and \mathbf{x} is

$$\tilde{A}(z, \mathbf{x}) \triangleq \sum_{k \in \mathcal{K}} x^*[k]y[k] \exp(j2\pi z d[k]/K). \quad (3)$$

Let the total power of the OFDM payload be $P = \sum_{k \in \mathcal{K}} x^*[k]x[k]$ and let the normalized received power at subcarrier k be $\rho[k] = x^*[k]x[k]/P$. The total integrated SNR is then defined as $\gamma \triangleq gP/\sigma^2$. When normalized by the channel gain and total power, the complex correlation in (3) becomes

$$\frac{1}{\sqrt{gP}} \tilde{A}(z, \mathbf{x}) = A(z, \boldsymbol{\rho}) + v_A(z, \mathbf{x}), \quad (4)$$

where $A(z, \boldsymbol{\rho})$ is the normalized complex ACF of the received signal without noise, and $v_A(z, \mathbf{x})$ is the noise component. These are defined as

$$A(z, \boldsymbol{\rho}) \triangleq \sum_{k \in \mathcal{K}} \rho[k] \exp(j2\pi(z - z_0)d[k]/K + j\phi_0), \quad (5)$$

$$v_A(z, \mathbf{x}) \triangleq \frac{1}{\sqrt{gP}} \sum_{k \in \mathcal{K}} x^*[k]v[k] \exp(j2\pi z d[k]/K). \quad (6)$$

It follows that $v_A(z, \mathbf{x}) \sim \mathcal{CN}(0, \gamma^{-1})$.

First consider the coherent reception case where the receiver knows ϕ_0 exactly. In this case, the maximum-likelihood estimator becomes [40]

$$\begin{aligned}\hat{z} &= \arg \max_z \Re\{\exp(-j\phi_0) \tilde{A}(z, \mathbf{x})\} \\ &= \arg \max_z A_C(z, \boldsymbol{\rho}) + \Re\{\exp(-j\phi_0) v_A(z, \mathbf{x})\},\end{aligned}\quad (7)$$

where $A_C(z, \boldsymbol{\rho}) \triangleq \Re\{\exp(-j\phi_0) A(z, \boldsymbol{\rho})\}$ is the normalized coherent ACF of the received signal without noise, simplifying to [17]

$$A_C(z, \boldsymbol{\rho}) = \sum_{k \in \mathcal{K}} \rho[k] \cos(2\pi z d[k]/K). \quad (8)$$

Next consider the noncoherent reception case where ϕ_0 is unknown. In this case, the maximum-likelihood estimator becomes [40]

$$\begin{aligned}\hat{z} &= \arg \max_z |\tilde{A}(z, \mathbf{x})|^2 \\ &= \arg \max_z A_N(z, \boldsymbol{\rho}) + 2\Re\{A^*(z, \boldsymbol{\rho}) v_A(z, \mathbf{x})\} + |v_A(z, \mathbf{x})|^2\end{aligned}\quad (9)$$

where $A_N(z, \boldsymbol{\rho}) \triangleq |A(z, \boldsymbol{\rho})|^2$ is the normalized noncoherent ACF of the received signal without noise:

$$\begin{aligned}A_N(z, \boldsymbol{\rho}) &= \left(\sum_{k \in \mathcal{K}} \rho[k] \cos(2\pi z d[k]/K) \right)^2 \\ &\quad + \left(\sum_{k \in \mathcal{K}} \rho[k] \sin(2\pi z d[k]/K) \right)^2.\end{aligned}\quad (10)$$

Both cases are of interest for radio positioning systems. The coherent detector minimizes the likelihood of detecting nearby sidelobes but may only be practical when the receiver's signal tracking has already obtained highly-accurate carrier phase measurements. Meanwhile, the noncoherent detector does not require *a priori* knowledge of the carrier phase, making it more applicable when accurate carrier phase measurements are not available. Much of the prior work on analyzing and optimizing the ZZB for TOA estimation has neglected to distinguish these two cases.

A. Estimation Error Bounds

Letting $\hat{\tau}$ be an unbiased estimate of τ_0 , the CRLB on TOA estimation error variance for OFDM signals is given by [11]

$$\begin{aligned}\mathbb{E}[(\hat{\tau} - \tau_0)^2] &\geq \sigma_{\text{CRLB}}^2(\boldsymbol{\rho}) \\ &\triangleq \left(8\pi^2 \gamma \Delta_f^2 \sum_{k \in \mathcal{K}} d^2[k] \rho[k] \right)^{-1}.\end{aligned}\quad (11)$$

The CRLB provides a valuable insight, namely, that estimator error variance scales inversely with the square of the distance (in frequency) of powered subcarriers from the carrier at the center of the band. Thus, a CRLB-optimal strategy would allocate all power to the extremes: $\rho[k] = 1/2$ for $k \in K/2 - 1, K/2$, otherwise $\rho[k] = 0$. However, the CRLB is only applicable at high SNR because it ignores the thresholding effects caused by sidelobes at lower SNR [16].

To resolve the shortcomings of the CRLB, the ZZB is computed to characterize the TOA error variance for a given OFDM pilot power allocation. This is preferred over the CRLB because it accounts for thresholding effects caused by sidelobes in the signal's ACF. The ZZB considers the error probability of a binary detection problem with equally-likely hypotheses: (1) the received signal experienced delay τ_0 , and (2) the received signal experienced delay $\tau_0 + \tau$. Assuming this error probability is shift-invariant, the hypotheses can be simplified without loss of generality by assuming $\tau_0 = 0$. The minimum probability of error for this problem is denoted $P_{\min}(z, \boldsymbol{\rho})$.

Assuming *a priori* knowledge that the TOA is uniformly distributed in $[0, T_a]$, the ZZB can be defined as [9], [13]

$$\begin{aligned}\mathbb{E}[(\hat{\tau} - \tau_0)^2] &\geq \sigma_{\text{ZZB}}^2(\boldsymbol{\rho}) \\ &\triangleq \frac{1}{T_a} \int_0^{T_a} \tau(T_a - \tau) P_{\min}(\tau/T_s, \boldsymbol{\rho}) d\tau \\ &= \frac{T_s^2}{N_a} \int_0^{N_a} z(N_a - z) P_{\min}(z, \boldsymbol{\rho}) dz,\end{aligned}\quad (12)$$

where $N_a \triangleq \frac{T_a}{T_s}$. Expressing the ZZB in this form with normalized time delays is useful since no terms in the integrand depend on the subcarrier spacing Δ_f , allowing the bound to be easily scaled to account for varying Δ_f .

As in the previous section, the receiver may perform either coherent or noncoherent detection, each having different error probabilities. The minimum probability of error for the coherent detector is [13], [41]

$$\begin{aligned}P_{\min, C}(z, \boldsymbol{\rho}) &= Q\left(\sqrt{\gamma(1 - A_C(z, \boldsymbol{\rho}))}\right) \\ &= \frac{1}{2} - \frac{1}{2} \operatorname{erf}\left(\sqrt{\frac{\gamma}{2}(1 - A_C(z, \boldsymbol{\rho}))}\right),\end{aligned}\quad (13)$$

and the resulting coherent ZZB is defined as

$$\sigma_{\text{ZZB}, C}^2(\boldsymbol{\rho}) \triangleq \frac{T_s^2}{N_a} \int_0^{N_a} z(N_a - z) P_{\min, C}(z, \boldsymbol{\rho}) dz. \quad (14)$$

Meanwhile, the minimum probability of error for the noncoherent detector is [41], [42]

$$P_{\min, N}(z, \boldsymbol{\rho}) = Q_1(a, b) - \frac{1}{2} \exp\left(\frac{-(a^2 + b^2)}{2}\right) I_0(ab), \quad (15)$$

$$a \triangleq \sqrt{\frac{\gamma}{2} \left(1 - \sqrt{1 - A_N(z, \boldsymbol{\rho})}\right)}, \quad (16)$$

$$b \triangleq \sqrt{\frac{\gamma}{2} \left(1 + \sqrt{1 - A_N(z, \boldsymbol{\rho})}\right)}, \quad (17)$$

and the resulting noncoherent ZZB is defined as

$$\sigma_{\text{ZZB}, N}^2(\boldsymbol{\rho}) \triangleq \frac{T_s^2}{N_a} \int_0^{N_a} z(N_a - z) P_{\min, N}(z, \boldsymbol{\rho}) dz. \quad (18)$$

It is important to note that neither the coherent nor noncoherent expressions for error probability depends on the phase of $x[k]$, only on the power $\rho[k]$ allocated to each subcarrier. The next section explores the optimization of the power allocations $\rho[k]$ to minimize the ZZB in both schemes.

III. OPTIMIZATION

A. Convex-Constrained Problem

ZZB-optimal OFDM power allocations can be found by minimizing the ZZB subject to a fixed power budget constraint. This optimization problem is written as

$$\begin{aligned} \min_{\boldsymbol{\rho}} \quad & \sigma_{\text{ZZB}}^2(\boldsymbol{\rho}) \\ \text{s.t.} \quad & \rho[k] \geq 0, \quad k \in \mathcal{K} \\ & \mathbf{1}^T \boldsymbol{\rho} - 1 = 0 \end{aligned} \quad (19)$$

where $\sigma_{\text{ZZB}}^2(\boldsymbol{\rho})$ is substituted with $\sigma_{\text{ZZB,C}}^2(\boldsymbol{\rho})$ for the coherent case or $\sigma_{\text{ZZB,N}}^2(\boldsymbol{\rho})$ for the noncoherent case. The affine equality constraint can be removed by expressing $\boldsymbol{\rho}$ as an affine function of a $K-1$ dimensional vector $\tilde{\boldsymbol{\rho}}$. Let $\tilde{\rho}[k] = \rho[k]$ for $k \in \tilde{\mathcal{K}}$, where $\tilde{\mathcal{K}} \triangleq \mathcal{K} \setminus \{0\}$ is the set of subcarrier indices excluding the DC subcarrier. Then define $\mathbf{F} \in \mathbb{R}^{K \times K-1}$ as $\mathbf{F} \triangleq [-\mathbf{1}, \mathbf{I}]^T$ and define $\mathbf{e}_0 \in \mathbb{R}^K$ as a one-hot vector with a 1 at index 0 and 0 elsewhere. Then, under the affine equality constraint, $\boldsymbol{\rho}$ can be parameterized as $\boldsymbol{\rho} = f(\tilde{\boldsymbol{\rho}}) \triangleq \mathbf{F}\tilde{\boldsymbol{\rho}} + \mathbf{e}_0$. The optimization problem in (19) can then be reframed as

$$\begin{aligned} \min_{\tilde{\boldsymbol{\rho}}} \quad & \sigma_{\text{ZZB}}^2(f(\tilde{\boldsymbol{\rho}})) \\ \text{s.t.} \quad & \tilde{\rho}[k] \geq 0, \quad k \in \tilde{\mathcal{K}} \\ & \mathbf{1}^T \tilde{\boldsymbol{\rho}} - 1 \leq 0 \end{aligned} \quad (20)$$

where the last inequality constraint arises from the inequality constraint on $\rho[0]$ in (19). Parameterizing the problem in this manner ensures that the gradients can be computed. Otherwise, the integrals for computing the gradients may diverge. The following section will prove that the optimization problem (19) is convex for both the coherent and noncoherent error probabilities. The following proof of convexity for the coherent case in Theorem 1 is different from the proof in [22] and demonstrates convexity with respect to OFDM subcarrier power allocations.

Theorem 1. *The coherent ZZB $\sigma_{\text{ZZB,C}}^2(\boldsymbol{\rho})$ is convex with respect to the OFDM power allocations $\boldsymbol{\rho}$ on the domain $\{\boldsymbol{\rho} \mid \mathbf{1}^T \boldsymbol{\rho} \leq 1, \rho[k] \geq 0\}$.*

Proof. For ease of expression, begin by defining

$$\lambda \triangleq A_C(z, \boldsymbol{\rho}), \quad (21)$$

resulting in

$$P_{\text{min,C}}(z, \boldsymbol{\rho}) = Q\left(\sqrt{\gamma(1-\lambda)}\right). \quad (22)$$

Note that $0 \leq \lambda \leq 1$. By Craig's formula [43], which is valid for $\sqrt{\gamma(1-\lambda)} \geq 0$ or equivalently $\lambda \leq 1$, $P_{\text{min,C}}(z, \boldsymbol{\rho})$ is rewritten as

$$\begin{aligned} P_{\text{min,C}}(z, \boldsymbol{\rho}) &= \frac{1}{\pi} \int_0^{\frac{\pi}{2}} \exp\left(\frac{-\gamma(1-\lambda)}{2\sin^2(\theta)}\right) d\theta \\ &= \lim_{\epsilon \rightarrow 0} \frac{1}{\pi} \int_{\epsilon}^{\frac{\pi}{2}} \exp\left(\frac{-\gamma}{2\sin^2(\theta)}\right) \exp\left(\frac{\gamma\lambda}{2\sin^2(\theta)}\right) d\theta \\ &= \lim_{\epsilon \rightarrow 0} \frac{1}{\pi} \int_{\epsilon}^{\frac{\pi}{2}} C_1(\theta) \exp(C_2(\theta)\lambda) d\theta. \end{aligned} \quad (23)$$

For any θ , it follows that $C_1(\theta) \geq 0$, $C_2(\theta) \geq 0$, and $\exp(C_2(\theta)\lambda)$ is convex with respect to λ . Since non-negative weighted integrals preserve convexity [44], $P_{\text{min,C}}(z, \boldsymbol{\rho})$ is convex with respect to λ . Recognizing that $A_C(z, \boldsymbol{\rho})$ is an affine mapping of $\boldsymbol{\rho}$ and that composition with an affine map preserves convexity [44], it follows that $P_{\text{min,C}}(z, \boldsymbol{\rho})$ is convex with respect to $\boldsymbol{\rho}$. Finally, the integral in (14) preserves convexity. Therefore $\sigma_{\text{ZZB,C}}^2(\boldsymbol{\rho})$, the ZZB defined in (14), is convex with respect to $\boldsymbol{\rho}$ on this domain. \square

This convexity is preserved under the affine mapping used to remove the equality constraint in (19), ensuring that (20) is also a convex problem. This convexity allows (20) to be efficiently solved using existing solvers. To aid the implementation of first and second order methods with these solvers, the gradient and Hessian of the ZZB with respect to the power allocations $\tilde{\boldsymbol{\rho}}$ are provided. When expressing the partial derivatives, the shorthand notation $\tilde{\rho}_n$ is substituted in place of $\tilde{\rho}[n]$.

The gradient of $P_{\text{min,C}}(z, f(\tilde{\boldsymbol{\rho}}))$ with respect to $\tilde{\boldsymbol{\rho}}$ is constructed of entries

$$\begin{aligned} \frac{\partial}{\partial \tilde{\rho}_n} P_{\text{min,C}}(z, f(\tilde{\boldsymbol{\rho}})) &= \frac{\sqrt{\gamma}}{2\sqrt{2\pi}} \exp\left(\frac{-\gamma}{2}(1 - A_C(z, f(\tilde{\boldsymbol{\rho}})))\right) \\ &\quad \times \frac{\cos(2\pi z d[n+1]/K) - 1}{\sqrt{1 - A_C(z, f(\tilde{\boldsymbol{\rho}}))}}. \end{aligned} \quad (24)$$

Similarly, the Hessian matrix of $P_{\text{min,C}}(z, f(\tilde{\boldsymbol{\rho}}))$ with respect to $\tilde{\boldsymbol{\rho}}$ is constructed of entries

$$\begin{aligned} \frac{\partial^2}{\partial \tilde{\rho}_n \partial \tilde{\rho}_m} P_{\text{min,C}}(z, f(\tilde{\boldsymbol{\rho}})) &= \frac{\sqrt{\gamma}}{4\sqrt{2\pi}} \exp\left(\frac{-\gamma}{2}(1 - A_C(z, f(\tilde{\boldsymbol{\rho}})))\right) \\ &\quad \times \frac{(\cos(2\pi z d[n+1]/K) - 1)(\cos(2\pi z d[m+1]/K) - 1)}{\sqrt{1 - A_C(z, \boldsymbol{\rho})}} \\ &\quad \times \left(\gamma + (1 - A_C(z, \boldsymbol{\rho}))^{-1}\right). \end{aligned} \quad (25)$$

The expressions for the gradient in (24) and Hessian in (25) are derived in Appendix A. Using (24), the gradient of the ZZB with respect to $\tilde{\boldsymbol{\rho}}$ can then be constructed with entries

$$\begin{aligned} \frac{\partial}{\partial \tilde{\rho}_n} \sigma_{\text{ZZB,C}}^2(f(\tilde{\boldsymbol{\rho}})) &= \frac{T_s^2}{N_a} \int_0^{N_a} z(N_a - z) \left(\frac{\partial}{\partial \tilde{\rho}_n} P_{\text{min,C}}(z, f(\tilde{\boldsymbol{\rho}}))\right) dz. \end{aligned} \quad (26)$$

Similarly using (25), the Hessian matrix of the ZZB with respect to $\tilde{\boldsymbol{\rho}}$ can be constructed with entries

$$\begin{aligned} \frac{\partial^2}{\partial \tilde{\rho}_n \partial \tilde{\rho}_m} \sigma_{\text{ZZB,C}}^2(f(\tilde{\boldsymbol{\rho}})) &= \frac{T_s^2}{N_a} \int_0^{N_a} z(N_a - z) \left(\frac{\partial^2}{\partial \tilde{\rho}_n \partial \tilde{\rho}_m} P_{\text{min,C}}(z, f(\tilde{\boldsymbol{\rho}}))\right) dz. \end{aligned} \quad (27)$$

Theorem 2. *The noncoherent ZZB $\sigma_{\text{ZZB,N}}^2(\boldsymbol{\rho})$ is convex with respect to the OFDM power allocations $\boldsymbol{\rho}$ on the domain $\{\boldsymbol{\rho} \mid \mathbf{1}^T \boldsymbol{\rho} \leq 1, \rho[k] \geq 0\}$.*

Proof. For ease of expression, begin by defining

$$\lambda \triangleq A_N(z, \boldsymbol{\rho}), \quad (28)$$

and note the following equivalences for a and b defined in (16) and (17) [42]:

$$\frac{a}{b} = \frac{\sqrt{\lambda}}{1 + \sqrt{1 - \lambda}}, \quad ab = \frac{\gamma}{2} \sqrt{\lambda}, \quad a^2 + b^2 = \frac{\gamma}{2}. \quad (29)$$

Then express the Marcum-Q function using its Neumann series expansion [45] as

$$Q_1(a, b) = \exp\left(\frac{-(a^2 + b^2)}{2}\right) \sum_{n=0}^{\infty} \left(\frac{a}{b}\right)^n I_{-n}(ab). \quad (30)$$

Recalling that $I_{-n}(\cdot) = I_n(\cdot)$ for integer values of n , this expansion can be substituted into $P_{\min, N}(z, \rho)$, resulting in

$$P_{\min, N}(z, \rho) = \frac{1}{2} \exp\left(\frac{-\gamma}{2}\right) \overbrace{I_0\left(\frac{\gamma}{2} \sqrt{\lambda}\right)}^A + \exp\left(\frac{-\gamma}{2}\right) \underbrace{\sum_{n=1}^{\infty} \left(\frac{\sqrt{\lambda}}{1 + \sqrt{1 - \lambda}}\right)^n I_n\left(\frac{\gamma}{2} \sqrt{\lambda}\right)}_B. \quad (31)$$

Note that the $n = 0$ term of the sum in (30) was combined with the original modified Bessel function term in (15). Since the exponential terms are positive, $P_{\min, N}(z, \rho)$ is a positive weighted sum of A and B and is convex if both A and B are convex. Now consider the series definition of the modified Bessel function of the first kind:

$$I_n(z) = \left(\frac{1}{2}z\right)^n \sum_{l=0}^{\infty} \frac{\left(\frac{1}{4}z^2\right)^l}{l! \Gamma(n + l + 1)} = \sum_{l=0}^{\infty} C_3(n, l) z^{2l+n}. \quad (32)$$

Then A can be expressed as

$$A = I_0\left(\frac{\gamma}{2} \sqrt{\lambda}\right) = \sum_{l=0}^{\infty} C_3(0, l) \lambda^l. \quad (33)$$

Since $C_3(0, l)$ is positive and λ^l is a convex function of λ for $0 \leq \lambda \leq 1$, it follows that A is convex with respect to λ for $0 \leq \lambda \leq 1$. Now B can be expressed as

$$B = \sum_{l=0}^{\infty} C_3(n, l) \left(\frac{\sqrt{\lambda}}{1 + \sqrt{1 - \lambda}}\right)^n \left(\frac{\gamma}{2}\right)^{2l+n} \lambda^{l+n/2} = \sum_{l=0}^{\infty} C_4(n, l) \left(1 + \sqrt{1 - \lambda}\right)^{-n} \lambda^{l+n}. \quad (34)$$

Both $(1 + \sqrt{1 - \lambda})^{-n}$ and λ^{l+n} are convex, nondecreasing, nonnegative, and bounded for all $0 \leq \lambda \leq 1$, $n \geq 1$, and $l \geq 0$. Since $C_4(n, l)$ is positive, it follows that B is convex for $0 \leq \lambda \leq 1$. Since both A and B are convex for $0 \leq \lambda \leq 1$, $P_{\min, N}(z, \rho)$ is convex with respect to λ on the domain $0 \leq \lambda \leq 1$. It also follows that $P_{\min, N}(z, \rho)$ is nondecreasing with respect to λ since both A and B are nondecreasing on this domain.

$P_{\min, N}(z, \rho)$ will now be shown to be convex with respect to $\rho[k]$ when $A_N(z, \rho)$ is substituted for λ and the power allocations are constrained to the convex domain

$\{\rho \mid \mathbf{1}^T \rho \leq 1, \rho[k] \geq 0\}$. On this domain, it follows that $0 \leq A_N(z, \rho) \leq 1$, which is a convex set equivalent to the domain on which $P_{\min, N}(z, \rho)$ was proven to be convex and nondecreasing with respect to $A_N(z, \rho)$. Additionally, $A_N(z, \rho)$ is a convex function of ρ . Therefore, by composition, $P_{\min, N}(z, \rho)$ is convex with respect to ρ on the domain $\{\rho \mid \mathbf{1}^T \rho \leq 1, \rho[k] \geq 0\}$. Finally, the integral in (18) preserves convexity. Therefore $\sigma_{\text{ZZB}, N}^2(\rho)$, the ZZB defined in (18), is convex with respect to ρ on this domain. \square

As in the coherent case, this convexity is preserved under the affine mapping used to remove the equality constraint in (19), ensuring that (20) is a convex problem. Gradients and Hessians may also be computed when solving the noncoherent form of (19). Due to its complexity, the Hessian for the noncoherent case is omitted in this paper, and first-order or quasi-Newton methods are recommended for solving the noncoherent optimization. The gradient of $P_{\min, N}(z, f(\tilde{\rho}))$ with respect to the power allocations $\tilde{\rho}$ is constructed of entries

$$\frac{\partial}{\partial \tilde{\rho}_n} P_{\min, N}(z, f(\tilde{\rho})) = \left(\frac{\partial}{\partial \tilde{\rho}_n} Q_1(a, b)\right) + \left(\frac{\partial}{\partial \tilde{\rho}_n} \frac{-1}{2} \exp\left(\frac{-\gamma}{2}\right) I_0(ab)\right), \quad (35)$$

whose terms are derived in detail in Appendix B. Using (35), the gradient of the ZZB with respect to $\tilde{\rho}$ can then be constructed with entries

$$\frac{\partial}{\partial \tilde{\rho}_n} \sigma_{\text{ZZB}, N}^2(f(\tilde{\rho})) = \frac{T_s^2}{N_a} \int_0^{N_a} z(N_a - z) \left(\frac{\partial}{\partial \tilde{\rho}_n} P_{\min, N}(z, f(\tilde{\rho}))\right) dz. \quad (36)$$

B. Integer-Constrained Problem

The results obtained from the optimization in (19) may not always be practical since power is allocated across the entire set of available subcarriers. In a dual-functional system, resources must also be allocated for communications purposes, and it may be preferable to multiplex these resources in frequency. Therefore, it is desirable to further constrain the optimization problem to the selection of a set of L subcarriers. The optimization problem is also further restricted to equal allocation of power across these L subcarriers, simplifying the optimization and avoiding narrowband interference concerns caused by allocating significant power into a small number of subcarriers. Under these constraints, the optimization problem can be written as

$$\begin{aligned} \min_{\rho} \quad & \sigma_{\text{ZZB}}^2(\rho) \\ \text{s.t.} \quad & \rho[k] \in \left\{0, \frac{1}{L}\right\}, \quad k \in \mathcal{K} \\ & \mathbf{1}^T \rho = 1 \end{aligned} \quad (37)$$

This is an NP-hard nonlinear integer programming problem. For any reasonable number of subcarriers K , a brute-force search is computationally prohibitive and requires evaluating $\binom{K}{L}$ selections. In light of these difficulties, a branch-and-bound algorithm [46] is proposed.

Recognizing that (19) is a convex relaxation of (37), the solutions to the convex-constrained problem in (19) serve as a lower bound to the integer-constrained problem in (37). Furthermore, the problem can be divided into subproblems in which certain binary decisions have already been made through the addition of equality constraints. In particular, consider two disjoint sets of subcarrier indices: $\mathcal{K}_0 \subseteq \mathcal{K}$ for which the power allocations are set to 0 and $\mathcal{K}_1 \subseteq \mathcal{K}$ for which the power allocations are set to $1/L$. For all subcarriers not included in either of these two sets, $k \in \mathcal{K} \setminus \mathcal{K}_0 \cup \mathcal{K}_1$, power allocations can be optimized without integer constraints to form a lower bound on each subproblem. Adding these equality constraints results in the relaxed subproblem

$$\begin{aligned} \min_{\boldsymbol{\rho}} \quad & \sigma_{\text{ZZB}}^2(\boldsymbol{\rho}) \\ \text{s.t.} \quad & \rho[k] \geq 0, \quad k \in \mathcal{K} \\ & \mathbf{1}^T \boldsymbol{\rho} = 1 \\ & \rho[k] = 0, \quad k \in \mathcal{K}_0 \\ & \rho[k] = \frac{1}{L}, \quad k \in \mathcal{K}_1 \end{aligned} \quad (38)$$

When $\mathcal{K}_0 \cup \mathcal{K}_1 = \emptyset$, this simplifies to (19), and when $|\mathcal{K}_1| > L$, the problem is infeasible. This relaxed subproblem allows the branch and bound algorithm to determine lower bounds on (37). Upper bounds on (37) are then found by evaluating the ZZB on a feasible approximation of the solutions of the relaxed subproblem in (38). These feasible approximations are found by setting the L subcarriers with the highest power allocations to a power of $1/L$ and setting all other subcarriers to a power of zero. This rounding function is denoted $\max_L(\boldsymbol{\rho})$.

With these upper and lower bounds, Algorithm 1 finds approximate solutions for (37). It adds subproblems to a priority queue, sorted such that subproblems with the smallest lower bound are popped first. Each subproblem has a relaxed solution $\check{\boldsymbol{\rho}}$, a lower bound $\check{\text{LB}}$ achieved by the relaxed solution, and constraint sets $\check{\mathcal{K}}_0$ and $\check{\mathcal{K}}_1$. In each iteration, a subproblem is popped from the queue and a subcarrier index k_b is selected for branching. Branching creates two additional subproblems: one where the power at subcarrier k_b is set to zero and one where the power at subcarrier k_b is set to $1/L$. For each subproblem, a relaxed solution $\boldsymbol{\rho}$, a lower bound LB , and an upper bound are computed. Each subproblem is then inserted into the priority queue so long as its lower bound is less than the tightest upper bound UB , after which the algorithm iterates. Since there are no guarantees that this algorithm converges to the optimal solution in fewer iterations than the brute force search, the iterations continue until either the optimality gap $\delta \triangleq (\text{UB} - \text{LB}) / \text{LB}$ is less than the tolerable gap δ_{tol} or the number of iterations exceeds N_{iter} .

IV. NUMERICAL RESULTS

A. Method and Setup

In a numerical demonstration, ZZB-optimal power allocations were found using both the convex-constrained problem (19) and the integer-constrained problem (37), and each problem was solved for both coherent reception, using the

Algorithm 1 Branch and Bound

Input: $N_{\text{iter}}, \delta_{\text{tol}}$
Output: $\boldsymbol{\rho}^*$

```

1:  $\mathcal{K}_0 \leftarrow \emptyset, \mathcal{K}_1 \leftarrow \emptyset$                                 ▷ Initialize
2:  $\boldsymbol{\rho} \leftarrow \text{Solution to (19)}$ 
3:  $\text{LB} \leftarrow \sigma_{\text{ZZB}}^2(\boldsymbol{\rho}), \text{UB} \leftarrow \sigma_{\text{ZZB}}^2(\max_L(\boldsymbol{\rho}))$ 
4:  $\boldsymbol{\rho}^* \leftarrow \max_L(\boldsymbol{\rho})$ 
5:  $\text{iter} \leftarrow 0, \delta \leftarrow \infty$ 
6: Insert  $\{\boldsymbol{\rho}, \text{LB}, \mathcal{K}_0, \mathcal{K}_1\}$  into PriorityQueue
7: while  $\text{iter} < N_{\text{iter}}$  or  $\delta < \delta_{\text{tol}}$  do
8:   Pop  $\{\check{\boldsymbol{\rho}}, \check{\text{LB}}, \check{\mathcal{K}}_0, \check{\mathcal{K}}_1\}$  from PriorityQueue
9:    $\delta = \frac{\text{UB} - \check{\text{LB}}}{\check{\text{LB}}}$ 
10:   $k_b = \arg \min_{k \in \mathcal{K} \setminus \{\check{\mathcal{K}}_0 \cup \check{\mathcal{K}}_1\}} |\check{\rho}[k] - \frac{1}{2L}|$   ▷ Branch
11:   $\mathcal{K}_0 \leftarrow \check{\mathcal{K}}_0 \cup \{k_b\}, \mathcal{K}_1 \leftarrow \check{\mathcal{K}}_1$           ▷ Subproblem 1
12:   $\boldsymbol{\rho} \leftarrow \text{Solution to (38)}$ 
13:   $\text{LB} \leftarrow \sigma_{\text{ZZB}}^2(\boldsymbol{\rho})$ 
14:  if  $\sigma_{\text{ZZB}}^2(\max_L(\boldsymbol{\rho})) < \text{UB}$  then
15:     $\text{UB} \leftarrow \sigma_{\text{ZZB}}^2(\max_L(\boldsymbol{\rho}))$ 
16:     $\boldsymbol{\rho}^* \leftarrow \max_L(\boldsymbol{\rho})$ 
17:  end if
18:  if  $\text{LB} < \text{UB}$  then
19:    Insert  $\{\boldsymbol{\rho}, \text{LB}, \mathcal{K}_0, \mathcal{K}_1\}$  into PriorityQueue
20:  end if
21:   $\mathcal{K}_0 \leftarrow \check{\mathcal{K}}_0, \mathcal{K}_1 \leftarrow \check{\mathcal{K}}_1 \cup \{k_b\}$           ▷ Subproblem 2
22:   $\boldsymbol{\rho} \leftarrow \text{Solution to (38)}$ 
23:   $\text{LB} \leftarrow \sigma_{\text{ZZB}}^2(\boldsymbol{\rho})$ 
24:  if  $\sigma_{\text{ZZB}}^2(\max_L(\boldsymbol{\rho})) < \text{UB}$  then
25:     $\text{UB} \leftarrow \sigma_{\text{ZZB}}^2(\max_L(\boldsymbol{\rho}))$ 
26:     $\boldsymbol{\rho}^* \leftarrow \max_L(\boldsymbol{\rho})$ 
27:  end if
28:  if  $\text{LB} < \text{UB}$  then
29:    Insert  $\{\boldsymbol{\rho}, \text{LB}, \mathcal{K}_0, \mathcal{K}_1\}$  into PriorityQueue
30:  end if
31:   $\text{iter} \leftarrow \text{iter} + 1$ 
32: end while

```

error probability in (13), and noncoherent reception, using the error probability in (15). These four variations of optimized allocations will be referred to as the coherent convex-optimized, coherent integer-optimized, noncoherent convex-optimized, and noncoherent integer-optimized allocations. For all problems, the OFDM signal was configured with $K = 64$ subcarriers and a subcarrier spacing of $\Delta_f = 15.625$ kHz, yielding a symbol duration of $64 \mu\text{s}$. The receiver's *a priori* TOA duration was $N_a = 16$ samples or $T_a = 16 \mu\text{s}$.

The coherent convex-constrained problem (19) was solved using an interior-point method using the analytical Jacobian and Hessian as provided by (26) and (27), iterating until convergence or a maximum of 30 iterations. The noncoherent version was solved similarly using the gradient in (36) and an approximate Hessian computed using BFGS [47].

The integer-constrained problem (37) was solved using the branch-and-bound algorithm as outlined in Algorithm 1, solving each relaxed subproblem (38) using an identical strategy as with the convex-constrained problem. The power allocations were restricted to $L = 8$ subcarriers. For both the coherent and noncoherent schemes, the branch-and-bound algorithm was configured with a tolerance $\delta_{\text{tol}} = 0.01$ and a maximum number of iterations $N_{\text{iter}} = 2000$.

Fig. 1 visualizes the resulting optimized power allocations across a range of SNRs. Fig. 1a shows the coherent convex-optimized allocations, Fig. 1b shows the coherent integer-

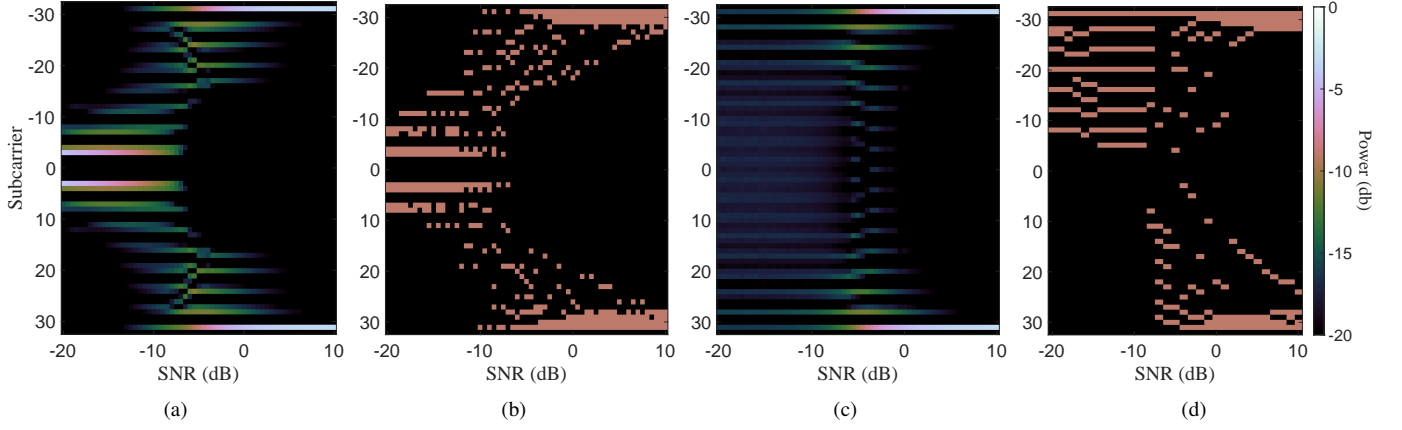


Fig. 1: The optimized subcarrier power allocations over a range of SNRs for the coherent convex-constrained problem (a), the coherent integer-constrained problem (b), the noncoherent convex-constrained problem (c), and the noncoherent integer-constrained problem (d). For the integer-constrained problems, $L = 8$.

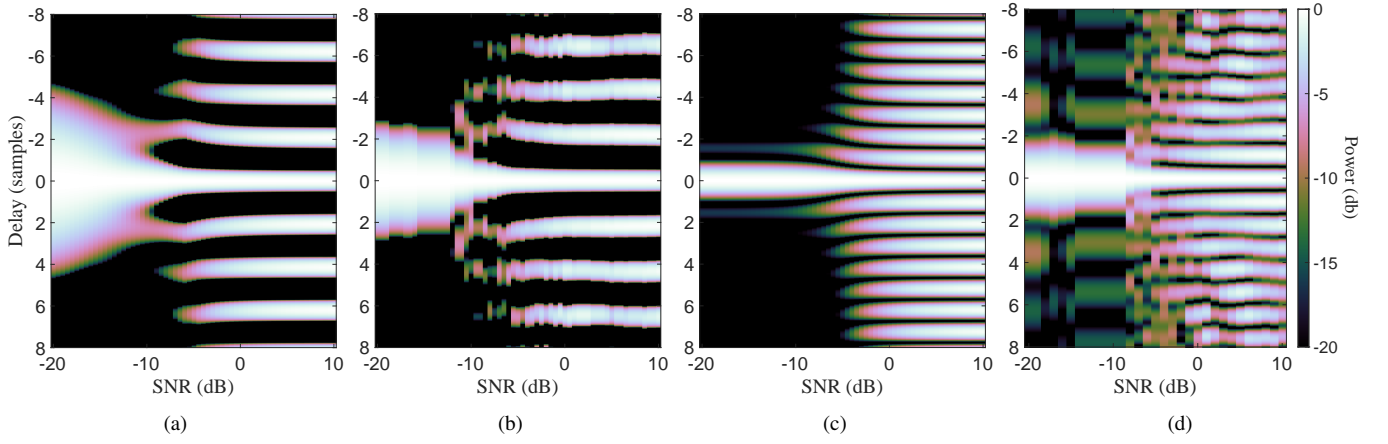


Fig. 2: The ACFs obtained from the allocations in Fig. 1 over a range of SNRs for the coherent convex-constrained problem (a), the coherent integer-constrained problem (b), the noncoherent convex-constrained problem (c), and the noncoherent integer-constrained problem (d). Negative values in the coherent ACFs are rounded up to -20 dB.

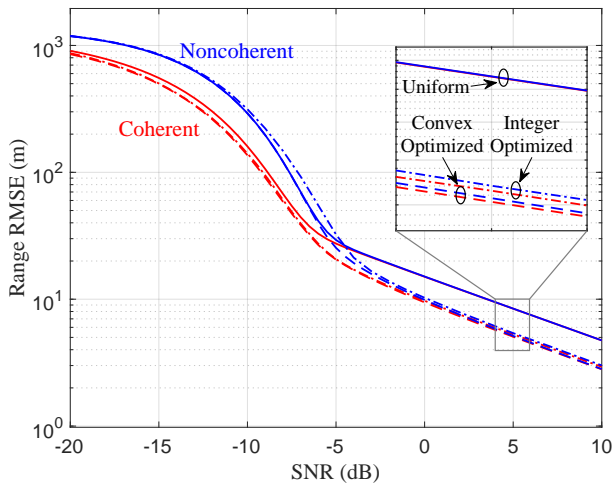


Fig. 3: The ZZB for the uniform allocation, convex-constrained optimized allocation, and the integer-constrained optimized allocation. Results are shown for both the coherent and noncoherent schemes.

optimized allocations, Fig. 1c shows the noncoherent convex-optimized allocations, and Fig. 1d shows the noncoherent integer-optimized allocations. The TOA ACFs obtained from these allocations are visualized in Fig. 2 in the same order. Fig. 3 plots the ZZB TOA root mean square errors (RMSEs) for all four variations and compares these against the coherent and noncoherent ZZBs obtained from a uniform power allocation across all subcarriers.

There are common trends seen in the optimal allocations and the resulting ACFs over the SNR range for all four variations. At low SNR, power is allocated in a manner that creates a wide mainlobe and minimizes sidelobes within the a priori TOA region. As SNR increases, sidelobes become more tolerable, allowing power to be allocated closer to the extremities of the spectrum to sharpen the mainlobe. At high SNR, the power allocation approaches the CRLB-optimal design of allocating all power to the outermost subcarriers yet maintains an appropriate amount of power in the inner subcarriers to prevent grating lobe ambiguities in the ACF. The ZZB is a powerfully general optimization criterion: it captures the transition from the low SNR regime to the high SNR regime.

B. Discussion

Consider the coherent and noncoherent cases in greater detail, starting with the coherent case, whose convex-optimized allocations are shown in Fig. 1a and whose integer-optimized allocations are shown in Fig. 1b. Due to the restrictions on subcarrier count and power, the integer-optimized allocations show a more gradual transition toward the CRLB-optimal choice of placing all power in the subcarrier extremities, placing power in a small number of central subcarriers to control sidelobe levels appropriately. Even with these constraints, the integer-optimized allocations create an ACF, shown in Fig. 2b, that closely resembles the convex-optimized ACF, shown in Fig. 2a. The branch-and-bound algorithm is capable of determining the best placement of these subcarriers while avoiding impractical brute-force searches. Moreover, Fig. 3 shows that the integer-optimized allocations achieve a ZZB that is negligibly worse than the ZZB achieved by the convex-optimized allocations over the entire SNR range. These are powerful results: near-optimal TOA performance can be achieved while only using a small fraction of the available spectral resources, allowing allocation of the unused subcarriers for communications or other purposes.

Next consider the noncoherent case. Fig. 1c visualizes the noncoherent convex-optimized allocations, which have a notably different distribution than the those in the coherent case shown in Fig. 1a. At low SNR, the power is distributed more uniformly across the spectrum, with approximately equal spacing between subcarriers containing significant power. This spacing permits grating lobe ambiguities in the ACF that fall outside of the *a priori* TOA duration. As SNR increases, the spacing shifts slightly and power is increasingly allocated to the outermost subcarriers. Fig. 2c shows the noncoherent ACFs of the optimized power allocations, depicting how these power allocations transition from minimal sidelobe levels at low SNR to minimal mainlobe width and tolerable sidelobes at high SNR. In contrast to the ACFs in Fig. 2a, many more sidelobes are present in Fig. 2c because sidelobes that previously took negative amplitudes in the coherent ACF take positive values in the noncoherent ACF. This increases the likelihood of sidelobe-dominated TOA errors and provides insight into the differences in optimal power allocation between coherent and noncoherent cases.

Fig. 1d visualizes the noncoherent integer-optimized allocations, which exhibit a unique structure. The noncoherent ACF has no dependence on the absolute placement of subcarriers within the spectrum and instead depends only on relative placements of subcarriers with respect to each other. This is in stark contrast to the coherent ACF which does factor in absolute subcarrier placement. Without loss of generality, the noncoherent integer-constrained problem was initialized with power placed in subcarrier -31 . At low SNR, the optimized power allocations take a sparse pattern which does not span the entire bandwidth. A rapid transition then occurs from -8 dB to -5 dB where the allocations expand to exploit the entire bandwidth. As SNR increases further, more power is allocated into the outermost subcarriers and fewer subcarriers are required in the center to maintain appropriate sidelobe

TABLE I: SDR Parameters

OFDM Parameters	
K	64 subcarriers
Δ_f (Subcarrier Spacing)	$\frac{3.125}{256}$ MHz
Symbol Duration	81.92 μ s
Cyclic Prefix Duration	40.96 μ s
Bandwidth	781.25 kHz
Measurement Parameters	
TX Gain	6 dB to 33 dB
RX Gain	10 dB
f_c (Carrier Frequency)	2.5 GHz
Digital Offset	781.25 kHz
Sample Rate	3.125 MS/s
z_0 (Relative Delay)	10.441 μ s
T_a (TOA Prior)	20.48 μ s
TX-RX Distance	~ 25 cm

levels. The transition toward allocating all power into the outermost subcarriers is slightly slower than that seen in the coherent integer-optimized allocations. Fig. 2d visualizes the noncoherent ACFs of these integer-optimized allocations. Unlike the previous variations, these ACFs have much higher sidelobes at low SNR, even compared against the coherent integer-optimized ACFs in Fig. 2b. This highlights the importance of using the noncoherent ZZB for optimization, as sidelobes are more difficult to control in the noncoherent case and coherent estimation may be infeasible at lower SNRs.

Fig. 3 quantifies the theoretical performance of the proposed optimized allocations for TOA estimation. In the coherent case, both the convex-optimized and integer-optimized allocations outperform the uniform allocation across the entire range of SNRs. Above -7 dB SNR, the optimized allocations achieve significantly reduced TOA RMSEs, ultimately reducing the TOA RMSE by up to 40% in the high SNR regime. The RMSE reduction continues into the low SNR regime, albeit less significantly, where the optimized allocations are able to exploit the receiver's *a priori* TOA knowledge. In the noncoherent case, the convex-optimized allocations achieve RMSEs similar to the uniform allocation's RMSEs in the low SNR regime but outperform the uniform allocation above -6 dB SNR. However, the noncoherent integer-optimized allocations experience an earlier thresholding effect below -4.5 dB and TOA errors increase faster than those with the uniform power allocation. This gap is explained by noting that the uniform allocation uses all 64 subcarriers as pilot resources, whereas the integer-optimized allocations only requires that 8 subcarriers be dedicated as pilot resources. In the high SNR regime, the noncoherent integer-optimized allocations achieve reduced TOA RMSEs that come close to the RMSEs achieved by the convex-optimized allocations.

V. EXPERIMENTAL RESULTS

In addition to the theoretical results in Sec. IV, the TOA estimation performance of the noncoherent optimized allocations was evaluated on an SDR measurement platform. Only the noncoherent allocations are evaluated because they do not require prior knowledge of the carrier phase, making these allocations more applicable to practical ranging systems.

A. Measurement Process

Experiments were conducted with two Ettus USRP N200s with synchronized clocks and timing. The transmit and receive antennas were spaced approximately 25 cm apart with an unobstructed line-of-sight propagation path. The parameters of the USRP devices are listed in Table I. The USRPs operated with direct conversion frontends, resulting in a strong DC component. To mitigate DC noise, the DC offset was calibrated prior to measurement and the OFDM signal was digitally offset by 781.25 kHz. The subcarrier noise variance $\hat{\sigma}^2$ was also measured from 1000 OFDM symbols sampled at the receiver USRP with the transmitter USRP off. The measurement process consisted of an SNR measurement stage and a TOA measurement stage.

In the SNR measurement stage, $M_{\text{SNR}} = 250$ OFDM symbols with a uniform pilot allocation are transmitted and received. After reception, the receiver USRP computes the complex correlation function as in (3) for all symbols, denoted for the m th symbol as $\tilde{A}_m(z, \mathbf{x})$ for $m = 0, 1, \dots, M_{\text{SNR}} - 1$. The receiver then estimates the integrated SNR from the peak power of the coherent sum of all complex correlation functions

$$\hat{\gamma} = \max_{z \in [0, N_a]} \frac{|\sum_{m=0}^{M_{\text{SNR}}} \tilde{A}_m(z, \mathbf{x})|^2}{\hat{\sigma}^2}. \quad (39)$$

The SNR can then be estimated as $\hat{\gamma}/K$.

In the TOA measurement stage, the transmitter selects the OFDM allocation optimized for an SNR closest to the estimated SNR and then transmits $M_{\text{TOA}} = 25 \times 10^3$ symbols generated from the chosen allocation. Similar to the SNR measurement stage, the receiver USRP then computes the complex correlation function, denoted for symbol m as $\tilde{A}_m(z, \mathbf{x})$ for $m = 0, 1, \dots, M_{\text{TOA}} - 1$. The receiver then estimates the TOA using the noncoherent estimator in (9), which is expressed in units of samples as

$$\hat{z}_m = \max_{z \in [0, N_a]} |\tilde{A}_m(z, \mathbf{x})|^2. \quad (40)$$

Prior to estimating the RMSE, the receiver discards the first $M_{\text{init}} = 50$ TOA estimates to eliminate any errors that could be caused by samples collected before the USRPs' RF components have settled to their tuning configuration. These measurements have a mean

$$\bar{z} = \frac{1}{M_{\text{TOA}} - M_{\text{init}}} \sum_{m=M_{\text{init}}}^{M_{\text{TOA}}-1} \hat{z}_m \quad (41)$$

and an unbiased RMSE

$$\hat{\sigma}_z = \sqrt{\frac{\sum_{m=M_{\text{init}}}^{M_{\text{TOA}}-1} (\hat{z}_m - \bar{z})^2}{M_{\text{TOA}} - M_{\text{init}} - 1}}. \quad (42)$$

This RMSE can be expressed in units of seconds by scaling $\hat{\sigma}_z$ by T_s or expressed in units of meters by scaling $\hat{\sigma}_z$ by cT_s , where c is the speed of light in m/s. This measurement process was repeated for transmit gains from 6 dB to 33 dB in intervals of 3 dB.

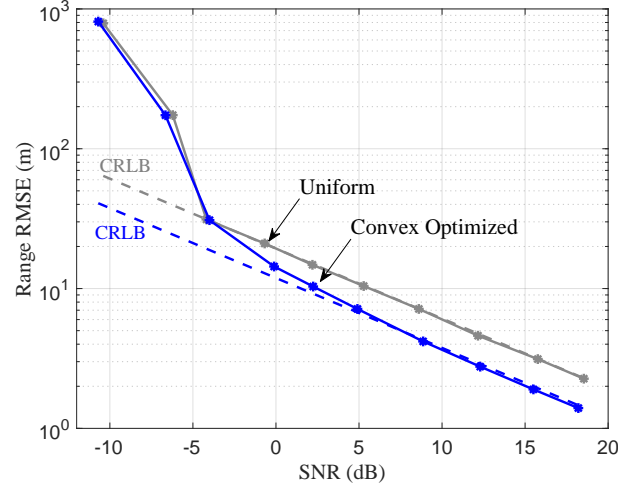


Fig. 4: Plots of the TOA RMSEs measured on the SDR platform using both the noncoherent optimized power allocation and a uniform power allocation. Results are compared against the CRLB.

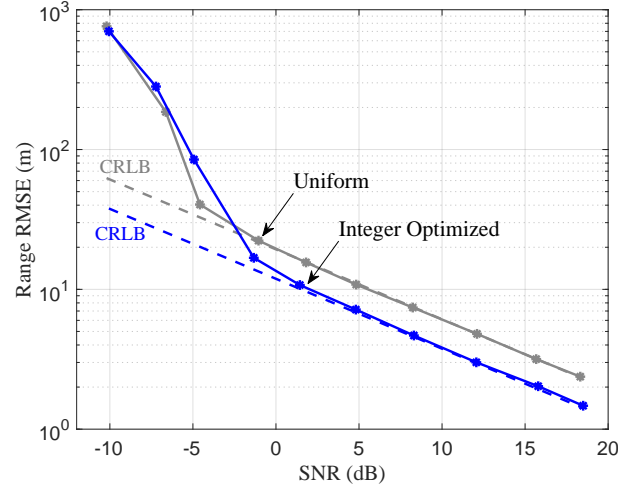


Fig. 5: Plots of the TOA RMSEs measured on the SDR platform using both the noncoherent integer-optimized power allocation and a uniform power allocation. Results are compared against the CRLB.

B. Measurement Results

Fig. 4 plots the measured RMSEs against the estimated SNRs collected on the SDR platform using both a uniform allocation and the noncoherent convex-optimized allocation. As in the theoretical results, the noncoherent convex-optimized allocation achieves an RMSE much better than the uniform allocation for moderate to high SNRs. Above 1 dB SNR, the measured RMSEs for both allocations closely follow their CRLBs.

Fig. 5 plots the measured RMSEs against the estimated SNRs collected on the SDR platform using both a uniform allocation and the noncoherent integer-optimized allocation. Compared to the convex-optimized allocation, the measured RMSE from the integer-optimized allocation diverges from the CRLB at a higher SNR and has greater errors than the

measured RMSE from the uniform allocation below approximately -3 dB SNR. This crossing point occurs at a slightly higher SNR than in the theoretical results, which is expected since the propagation channel is not an ideal AWGN channel in practice. Despite its worse performance at low SNR, the integer-optimized allocation may be a desirable allocation since it only requires 8 pilot subcarriers, allowing data or other resources to be multiplexed in frequency unlike the uniform allocation which requires all 64 subcarriers.

VI. CONCLUSIONS

This paper has demonstrated how OFDM pilot allocations can be optimized to minimize TOA estimation errors in a manner that accounts for the low SNR thresholding effects caused by the presence of sidelobes in the signal's ACF. This optimization was conducted by minimizing the ZZB and was analyzed under both coherent and noncoherent reception. This paper proved the convexity of the problem, provided readily-usable expressions for the gradients, and solved for optimal allocations over a wide range of SNRs. The theoretical TOA error variances achieved by the optimal allocations were compared against the error variances achieved by a uniform allocation. Integer constraints were then introduced into the optimization problem, in which the pilot allocations are restricted to a sparse selection of subcarriers with equally-distributed power. A branch-and-bound algorithm was proposed for solving this integer-constrained problem to achieve near-optimal allocations that only require a sparse subset of subcarriers, solving for these allocations over a wide range of SNRs and comparing the theoretical TOA error variances against uniform allocations. The real-world applicability of these pilot allocations was demonstrated by measuring the TOA errors obtained from SDRs transmitting and receiving the optimized signals.

These results illustrate how intelligent allocation of pilot resources within OFDM signals can yield notable improvements in TOA estimation, even when constrained to using a sparse subset of subcarriers. Such optimal allocations will be a key enabler of dual-functional and ISAC systems that aim to achieve precise TOA-based user positioning with a minimal number of resources allocated for positioning, freeing up resources for communications.

ACKNOWLEDGMENTS

This work was supported by the U.S. Space Force under an STTR contract with Coherent Technical Services, Inc., and by affiliates of the 6G@UT center within the Wireless Networking and Communications Group at The University of Texas at Austin.

APPENDIX A COHERENT ERROR PROBABILITY GRADIENT AND HESSIAN

First, the gradients of the coherent probability of error $P_{\min,C}(z, f(\tilde{\rho}))$ with respect to the mapped power allocations

$\tilde{\rho}$, expressed in (24), will be derived. Taking the partial derivatives of (13) yields

$$\begin{aligned} & \frac{\partial}{\partial \tilde{\rho}_n} P_{\min,C}(z, f(\tilde{\rho})) \\ &= \frac{\partial}{\partial \tilde{\rho}_n} \frac{1}{2} - \frac{1}{2} \operatorname{erf} \left(\sqrt{\frac{\gamma}{2}} (1 - A_C(z, f(\tilde{\rho}))) \right) \\ &= \frac{\partial}{\partial \tilde{\rho}_n} \frac{1}{2} - \frac{1}{\sqrt{\pi}} \int_0^{\sqrt{\frac{\gamma}{2}} (1 - A_C(z, f(\tilde{\rho})))} \exp(-t^2) dt \\ &= \frac{-1}{\sqrt{\pi}} \exp \left(\frac{-\gamma}{2} (1 - A_C(z, f(\tilde{\rho}))) \right) \\ &\quad \times \left(\frac{\partial}{\partial \tilde{\rho}_n} \sqrt{\frac{\gamma}{2}} (1 - A_C(z, f(\tilde{\rho}))) \right) \\ &= \frac{-1}{2\sqrt{\pi}} \exp \left(\frac{-\gamma}{2} (1 - A_C(z, f(\tilde{\rho}))) \right) \frac{\frac{\partial}{\partial \tilde{\rho}_n} \frac{-\gamma}{2} A_C(z, f(\tilde{\rho}))}{\sqrt{\frac{\gamma}{2}} (1 - A_C(z, f(\tilde{\rho})))} \\ &= \frac{\sqrt{\gamma}}{2\sqrt{2\pi}} \exp \left(\frac{-\gamma}{2} (1 - A_C(z, f(\tilde{\rho}))) \right) \frac{\cos(2\pi z d[n+1]/K) - 1}{\sqrt{1 - A_C(z, f(\tilde{\rho}))}} \end{aligned} \quad (43)$$

Next, the Hessian of $P_{\min,C}(z, f(\tilde{\rho}))$ with respect to $\tilde{\rho}$ is derived. Taking the partial derivatives of (43) yields

$$\begin{aligned} & \frac{\partial^2}{\partial \tilde{\rho}_n \partial \tilde{\rho}_m} P_{\min,C}(z, f(\tilde{\rho})) \\ &= \frac{\partial}{\partial \tilde{\rho}_m} \overbrace{\frac{\sqrt{\gamma}}{2\sqrt{2\pi}} \exp \left(\frac{-\gamma}{2} (1 - A_C(z, f(\tilde{\rho}))) \right)}^{A_2} \\ &\quad \times \underbrace{\frac{\cos(2\pi z d[n+1]/K) - 1}{\sqrt{1 - A_C(z, f(\tilde{\rho}))}}}_{B_2} \\ &= \left(\frac{\partial}{\partial \tilde{\rho}_m} A_2 \right) B_2 + A_2 \left(\frac{\partial}{\partial \tilde{\rho}_m} B_2 \right). \end{aligned} \quad (44)$$

The partial derivatives of A_2 and B_2 are

$$\begin{aligned} \frac{\partial}{\partial \tilde{\rho}_m} A_2 &= \frac{\gamma^{3/2}}{4\sqrt{2\pi}} \exp \left(\frac{-\gamma}{2} (1 - A_C(z, f(\tilde{\rho}))) \right) \\ &\quad \times (\cos(2\pi z d[m+1]/K) - 1), \end{aligned} \quad (45)$$

and

$$\begin{aligned} & \frac{\partial}{\partial \tilde{\rho}_m} B_2 \\ &= \frac{-(\cos(2\pi z d[n+1]/K) - 1)(\cos(2\pi z d[m+1]/K) - 1)}{2(1 - A_C(z, f(\tilde{\rho})))^{3/2}}. \end{aligned} \quad (46)$$

Through some algebra, (44) becomes

$$\begin{aligned} & \frac{\partial^2}{\partial \tilde{\rho}_n \partial \tilde{\rho}_m} P_{\min,C}(z, f(\tilde{\rho})) \\ &= \frac{\sqrt{\gamma}}{4\sqrt{2\pi}} \exp \left(\frac{-\gamma}{2} (1 - A_C(z, f(\tilde{\rho}))) \right) \\ &\quad \times \frac{(\cos(2\pi z d[n+1]/K) - 1)(\cos(2\pi z d[m+1]/K) - 1)}{\sqrt{1 - A_C(z, f(\tilde{\rho}))}} \\ &\quad \times \left(\gamma + (1 - A_C(z, f(\tilde{\rho})))^{-1} \right). \end{aligned} \quad (47)$$

APPENDIX B

NONCOHERENT ERROR PROBABILITY GRADIENT

The gradients of the noncoherent probability of error $P_{\min,N}(z, f(\tilde{\rho}))$ with respect to the mapped power allocations $\tilde{\rho}$, expressed in (35), are derived. Through application of the multivariable chain rule, the partial derivatives of the Marcum-Q term are

$$\begin{aligned} \frac{\partial}{\partial \tilde{\rho}_n} Q_1(a, b) &= \left(\frac{\partial}{\partial \tilde{\rho}_n} a \right) \left(\frac{\partial}{\partial a} Q_1(a, b) \right) \\ &+ \left(\frac{\partial}{\partial \tilde{\rho}_n} b \right) \left(\frac{\partial}{\partial b} Q_1(a, b) \right). \end{aligned} \quad (48)$$

The partial derivatives of the Marcum-Q with respect to its inputs a and b are [45]

$$\frac{\partial}{\partial a} Q_1(a, b) = b \exp(-\gamma/2) I_1(ab), \quad (49)$$

$$\frac{\partial}{\partial b} Q_1(a, b) = -b \exp(-\gamma/2) I_0(ab), \quad (50)$$

while the partial derivatives of a and b with respect to $\tilde{\rho}$ are

$$\frac{\partial}{\partial \tilde{\rho}_n} a = \frac{\frac{\sqrt{\gamma}}{4\sqrt{2}} \left(\frac{\partial}{\partial \tilde{\rho}_n} A_N(z, f(\tilde{\rho})) \right)}{\sqrt{1 - A_N(z, f(\tilde{\rho}))} \sqrt{1 - \sqrt{1 - A_N(z, f(\tilde{\rho}))}}}, \quad (51)$$

$$\frac{\partial}{\partial \tilde{\rho}_n} b = \frac{\frac{-\sqrt{\gamma}}{4\sqrt{2}} \left(\frac{\partial}{\partial \tilde{\rho}_n} A_N(z, f(\tilde{\rho})) \right)}{\sqrt{1 - A_N(z, f(\tilde{\rho}))} \sqrt{1 + \sqrt{1 - A_N(z, f(\tilde{\rho}))}}}. \quad (52)$$

The partial derivatives of the noncoherent autocorrelation function with respect to $\tilde{\rho}$ are

$$\begin{aligned} \frac{\partial}{\partial \tilde{\rho}_n} A_N(z, f(\tilde{\rho})) &= \sum_{k=0}^{K-2} 2\tilde{\rho}[k] (\cos(2\pi z d[k+1]/K) - 1) \cos(2\pi z d[n+1]/K) \\ &+ \sum_{k=0}^{K-2} 2\tilde{\rho}[k] \sin(2\pi z d[k+1]/K) \sin(2\pi z d[n+1]/K). \end{aligned} \quad (53)$$

Simple substitution of (48-53) yields the gradients of the Marcum-Q term in (35). Next, the partial derivatives of the modified Bessel function term in (35) are

$$\begin{aligned} \frac{\partial}{\partial \tilde{\rho}_n} \frac{-1}{2} \exp\left(\frac{-\gamma}{2}\right) I_0(ab) &= \frac{\partial}{\partial \tilde{\rho}_n} \frac{-1}{2} \exp\left(\frac{-\gamma}{2}\right) I_0\left(\frac{\gamma}{2} \sqrt{A_N(z, f(\tilde{\rho}))}\right) \\ &= \frac{-1}{2} \exp\left(\frac{-\gamma}{2}\right) I_1\left(\frac{\gamma}{2} \sqrt{A_N(z, f(\tilde{\rho}))}\right) \frac{\gamma \left(\frac{\partial}{\partial \tilde{\rho}_n} A_N(z, f(\tilde{\rho})) \right)}{4\sqrt{A_N(z, f(\tilde{\rho}))}}. \end{aligned} \quad (54)$$

Finally, the expressions for (48) and (54) can be substituted into (35) to obtain the desired gradient of $P_{\min,N}(z, f(\tilde{\rho}))$.

REFERENCES

- [1] K. Shamaei, J. Khalife, and Z. M. Kassas, "Exploiting LTE signals for navigation: Theory to implementation," *IEEE Transactions on Wireless Communications*, vol. 17, no. 4, pp. 2173–2189, 2018.
- [2] S. Dwivedi, R. Shreevastav, F. Munier, J. Nygren, I. Siomina, Y. Lyazidi, D. Shrestha, G. Lindmark, P. Ernström, E. Stare *et al.*, "Positioning in 5G networks," *IEEE Communications Magazine*, vol. 59, no. 11, pp. 38–44, 2021.
- [3] C. R. Berger, B. Demissie, J. Heckenbach, P. Willett, and S. Zhou, "Signal processing for passive radar using OFDM waveforms," *IEEE Journal of Selected Topics in Signal Processing*, vol. 4, no. 1, pp. 226–238, 2010.
- [4] A. Zeira and P. M. Schultheiss, "Realizable lower bounds for time delay estimation. 2. Threshold phenomena," *IEEE transactions on signal processing*, vol. 42, no. 5, pp. 1001–1007, 1994.
- [5] J. A. Nanzer, M. D. Sharp, and D. Richard Brown, "Bandpass signal design for passive time delay estimation," in *2016 50th Asilomar Conference on Signals, Systems and Computers*, Nov. 2016, pp. 1086–1091.
- [6] Z. Sahinoglu, S. Gezici, and I. Güvenc, *Ultra-wideband positioning systems: theoretical limits, ranging algorithms, and protocols*. Cambridge university press, 2008.
- [7] E. W. Barankin, "Locally best unbiased estimates," *The Annals of Mathematical Statistics*, vol. 20, no. 4, pp. 477–501, 1949. [Online]. Available: <http://www.jstor.org/stable/2236306>
- [8] R. McAulay and E. Hofstetter, "Barankin bounds on parameter estimation," *IEEE Transactions on Information Theory*, vol. 17, no. 6, pp. 669–676, 1971.
- [9] J. Ziv and M. Zakai, "Some lower bounds on signal parameter estimation," *IEEE Transactions on Information Theory*, vol. 15, no. 3, pp. 386–391, 1969.
- [10] J. A. del Peral-Rosado, J. A. López-Salcedo, F. Zanier, and G. Seco-Granados, "Position accuracy of joint time-delay and channel estimators in LTE networks," *IEEE Access*, vol. 6, pp. 25 185–25 199, 2018.
- [11] W. Xu, M. Huang, C. Zhu, and A. Dammann, "Maximum likelihood TOA and OTDOA estimation with first arriving path detection for 3GPP LTE system," *Transactions on Emerging Telecommunications Technologies*, vol. 27, no. 3, pp. 339–356, 2016.
- [12] N. Liu, Z. Xu, and B. M. Sadler, "Ziv-Zakai time-delay estimation bounds for frequency-hopping waveforms under frequency-selective fading," *IEEE transactions on signal processing*, vol. 58, no. 12, pp. 6400–6406, 2010.
- [13] D. Dardari and M. Z. Win, "Ziv-Zakai bound on time-of-arrival estimation with statistical channel knowledge at the receiver," in *2009 IEEE International Conference on Ultra-Wideband*. IEEE, 2009, pp. 624–629.
- [14] A. Gusi-Amigó, P. Closas, A. Mallat, and L. Vandendorpe, "Ziv-Zakai bound for direct position estimation," *Navigation*, vol. 65, no. 3, pp. 463–475, 2018.
- [15] Z. Zhang, C. Zhou, C. Yan, and Z. Shi, "Deterministic Ziv-Zakai bound for compressive time delay estimation," in *2022 IEEE Radar Conference (RadarConf22)*. IEEE, 2022, pp. 1–5.
- [16] A. M. Graff and T. E. Humphreys, "Purposeful co-design of OFDM signals for ranging and communications," *EURASIP Journal on Advances in Signal Processing*, 2024.
- [17] T. Laas and W. Xu, "On the Ziv-Zakai bound for time difference of arrival estimation in CP-OFDM systems," in *2021 IEEE Wireless Communications and Networking Conference (WCNC)*. IEEE, 2021, pp. 1–5.
- [18] A. Dammann, T. Jost, R. Raulefs, M. Walter, and S. Zhang, "Optimizing waveforms for positioning in 5G," in *2016 IEEE 17th International Workshop on Signal Processing Advances in Wireless Communications (SPAWC)*. IEEE, 2016, pp. 1–5.
- [19] E. Staudinger, M. Walter, and A. Dammann, "Optimized waveform for energy efficient ranging," in *2017 14th Workshop on Positioning, Navigation and Communications (WPNC)*. IEEE, 2017, pp. 1–6.
- [20] M. Driusso, M. Comisso, F. Babich, and C. Marshall, "Performance analysis of time of arrival estimation on OFDM signals," *IEEE Signal Processing Letters*, vol. 22, no. 7, pp. 983–987, 2015.
- [21] M. Wirsing, A. Dammann, and R. Raulefs, "Designing a ranging signal for use with VDE R-mode," in *2020 IEEE/ION Position, Location and Navigation Symposium (PLANS)*. IEEE, 2020, pp. 822–826.
- [22] Y. Xiong and F. Liu, "SNR-adaptive ranging waveform design based on Ziv-Zakai bound optimization," *IEEE Signal Processing Letters*, 2023.
- [23] J. Sun, S. Ma, G. Xu, and S. Li, "Trade-off between positioning and communication for millimeter wave systems with Ziv-Zakai bound," *IEEE Transactions on Communications*, 2023.
- [24] H. Dun, C. C. Tiberius, C. E. Diouf, and G. J. Janssen, "Design of sparse multiband signal for precise positioning with joint low-complexity time delay and carrier phase estimation," *IEEE Transactions on Vehicular Technology*, vol. 70, no. 4, pp. 3552–3567, 2021.
- [25] Y. Karisan, D. Dardari, S. Gezici, A. A. D'Amico, and U. Mengali, "Range estimation in multicarrier systems in the presence of interference: Performance limits and optimal signal design," *IEEE Transactions on Wireless Communications*, vol. 10, no. 10, pp. 3321–3331, 2011.

- [26] M. D. Larsen, G. Seco-Granados, and A. L. Swindlehurst, "Pilot optimization for time-delay and channel estimation in OFDM systems," in *2011 IEEE International Conference on Acoustics, Speech and Signal Processing (ICASSP)*, 2011, pp. 3564–3567.
- [27] R. Montalbán, J. A. López-Salcedo, G. Seco-Granados, and A. L. Swindlehurst, "Power allocation approaches for combined positioning and communications OFDM systems," in *2013 IEEE 14th Workshop on Signal Processing Advances in Wireless Communications (SPAWC)*. IEEE, 2013, pp. 694–698.
- [28] Y. Li, Z. Wei, and Z. Feng, "Joint subcarrier and power allocation for uplink integrated sensing and communication system," *IEEE Sensors Journal*, 2023.
- [29] M. Jamalabdollahi and S. R. Zekavat, "High resolution ToA estimation via optimal waveform design," *IEEE Transactions on Communications*, vol. 65, no. 3, pp. 1207–1218, 2017.
- [30] A. Gupta, U. Madhow, A. Arbabian, and A. Sadri, "Design of large effective apertures for millimeter wave systems using a sparse array of subarrays," *IEEE Transactions on Signal Processing*, vol. 67, no. 24, pp. 6483–6497, 2019.
- [31] V. M. Chiriac, Q. He, A. M. Haimovich, and R. S. Blum, "Ziv-Zakai bound for joint parameter estimation in MIMO radar systems," *IEEE Transactions on Signal Processing*, vol. 63, no. 18, pp. 4956–4968, 2015.
- [32] F. Liu, Y. Cui, C. Masouros, J. Xu, T. X. Han, Y. C. Eldar, and S. Buzzi, "Integrated sensing and communications: Toward dual-functional wireless networks for 6G and beyond," *IEEE journal on selected areas in communications*, vol. 40, no. 6, pp. 1728–1767, 2022.
- [33] Y. Liu, G. Liao, J. Xu, Z. Yang, and Y. Zhang, "Adaptive OFDM integrated radar and communications waveform design based on information theory," *IEEE Communications Letters*, vol. 21, no. 10, pp. 2174–2177, 2017.
- [34] Z. Zhang, Z. Du, and W. Yu, "Mutual-information-based OFDM waveform design for integrated radar-communication system in Gaussian mixture clutter," *IEEE Sensors Letters*, vol. 4, no. 1, pp. 1–4, 2019.
- [35] Z. Wei, J. Piao, X. Yuan, H. Wu, J. A. Zhang, Z. Feng, L. Wang, and P. Zhang, "Waveform design for mimo-ofdm integrated sensing and communication system: An information theoretical approach," *IEEE Transactions on Communications*, 2023.
- [36] S. D. Liyanaarachchi, C. B. Barneto, T. Riihonen, and M. Valkama, "Joint OFDM waveform design for communications and sensing convergence," in *ICC 2020-2020 IEEE International Conference on Communications (ICC)*. IEEE, 2020, pp. 1–6.
- [37] F. Wang, H. Li, and M. A. Govoni, "Power allocation and co-design of multicarrier communication and radar systems for spectral coexistence," *IEEE Transactions on Signal Processing*, vol. 67, no. 14, pp. 3818–3831, 2019.
- [38] Z. Ni, J. A. Zhang, K. Yang, X. Huang, and T. A. Tsiftsis, "Multi-metric waveform optimization for multiple-input single-output joint communication and radar sensing," *IEEE Transactions on Communications*, vol. 70, no. 2, pp. 1276–1289, 2021.
- [39] S. Sen, G. Tang, and A. Nehorai, "Multiobjective optimization of OFDM radar waveform for target detection," *IEEE Transactions on Signal Processing*, vol. 59, no. 2, pp. 639–652, 2010.
- [40] D. Rife and R. Boorstyn, "Single tone parameter estimation from discrete-time observations," *IEEE Transactions on information theory*, vol. 20, no. 5, pp. 591–598, 1974.
- [41] J. Proakis and M. Salehi, *Digital communications 5th Edition*. McGraw-Hill, 2007.
- [42] C. W. Helstrom, "The resolution of signals in white, Gaussian noise," *Proceedings of the IRE*, vol. 43, no. 9, pp. 1111–1118, 1955.
- [43] J. W. Craig, "A new, simple and exact result for calculating the probability of error for two-dimensional signal constellations," in *MILCOM 91-Conference record*. IEEE, 1991, pp. 571–575.
- [44] S. P. Boyd and L. Vandenberghe, *Convex optimization*. Cambridge university press, 2004.
- [45] A. Annamalai and C. Tellambura, "A simple exponential integral representation of the generalized marcum Q-function $QM(a,b)$ for real-order M with applications," in *MILCOM 2008-2008 IEEE Military Communications Conference*. IEEE, 2008, pp. 1–7.
- [46] H. Tuy, T. Hoang, T. Hoang, V.-n. Mathématicien, T. Hoang, and V. Mathématician, *Convex analysis and global optimization*. Springer, 1998.
- [47] R. Fletcher, *Practical methods of optimization*. John Wiley & Sons, 2000.